Romanian Reports in Physics **72**, 202 (2020)

COMPETITION BETWEEN ^{296}Lv α DECAY AND FISSION AS FUNCTION OF THE EXCITATION ENERGY

M. MIREA[1,2], A. SANDULESCU[1,2,3*]

[1]Department of Theoretical Physics,
National Institute for Physics and Nuclear Engineering "Horia Hulubei",
Atomistilor 407, RO-077125, POB-MG6, Măgurele-Bucharest, Romania
Email: *mirea@theory.nipne.ro*
[2]Academy of Romanian Scientists,
Splaiul Independentei 54, 050094 Bucharest, Romania
[3]Romanian Academy, Calea Victoriei 125, Bucharest, Romania

Received April 20, 2020

Abstract. The deformation energy for the ^{296}Lv superheavy element is calculated in the framework of the macroscopic-microscopic model based on the the Woods-Saxon two-center shell model. The inertia is obtained within the cranking approach. The superasymmetric fission and the near symmetric fission of ^{296}Lv nucleus are investigated. The fission paths are obtained by minimizing the action integral constrained by a final configuration pertaining to the fission or to the α decay process. In both cases, the potential barrier exhibits a two-humped structure characterized by a deep second well. The ratio between α-decay and cold fission decay probabilities are reported for different excitation energies of the parent nucleus.

Key words: Fission, α decay, Superheavy elements.

1. INTRODUCTION

It is well known that ^{48}Ca is one of the most employed projectiles used in combination with different heavy targets for the synthesis of superheavy elements. This optimum projectile/target combination that leads to cold fusion reactions was predicted in Ref. [1]. An appropriate method for the optimum choice of the reaction partners for the synthesis of superheavy elements was inferred in the framework of the fragmentation theory. A complicated shell effects structure of the multidimensional potential energy surface is exhibited within the the Strutinsky prescriptions, evidencing some valleys in the mass-asymmetry coordinate. The interacting fragments should have a minimal excitation energy along the valley when the compound system is formed. Thus, the largest survival probability of the compound nucleus corresponds to ^{48}Ca projectile as a optimum candidate. Using the microscopic-macroscopic method and the superasymmetric two-center shell model based on harmonic oscillators, an extended analysis of all possible combinations highlighted

*Deceased 21 April 2019

[2–4] that the most favorable channels able to produce isotopes with $Z \geq 104$ are connected with the so-called ^{208}Pb potential valley, *i.e.* the same valley as that of the heavy cluster emission [5]. By assuming that a ^{208}Pb similar valley exists for ^{48}Ca, in Ref. [3], the ^{48}Ca was proposed as a projectile on various transuranium targets. This prediction was proved of crucial importance during the last three decades, having in mind that the production of many superheavy elements with $Z \leq 118$ was mainly based on this idea [6–12]. Other options for superheavy element synthesis were tested experimentally by using ^{45}Cr, ^{64}Ni or ^{58}Fe beams [13, 14]. For the last isotopes, it was found that the fast fission channel becomes the most important one and the survival probability for the superheavy element drops by several orders of magnitude. In the following, the previous work is developed by using a more realistic two center shell model and by extending the investigation of the potential energy surface, aiming to understand better the behavior of the cold fusion as a many-body process. Based on the above mentioned arguments, the $^{296}_{116}$Lv superheavy element synthesis was studied, obtained in the reaction ^{248}Cm+^{48}Ca. Recently, the existence of a valley in the deformation energy was assessed for the α-decay [15]. Within the same model, the α-decay, the cluster emission, the fission, and the synthesis of superheavy elements were described in an unitary manner. In Ref. [15], we used the following even-even combinations of light nuclei and their partners that give the compound ^{296}Lv superheavy element: ^{4,6}He, ^{8,10}Be, ^{12,14}C, ^{16,20}O, ^{22,24}Ne, ^{26,28,30}Mg, ^{32,34,36}Si, ^{38,40,42}S, ^{44,46}Ar, ^{48,50}Ca, ^{52,54}Ti, ^{56,58}Cr, $^{62-64}$Fe, ^{66,68,70}Ni, ^{72,74,76}Zn, ^{78,82}Ge, ^{80}Zr, ^{84,86,88}Se, $^{90.92.94}$Kr, ^{96,98,100}Sr, ^{102}Zr, ^{104,106,108}Mo, ^{110,112,114}Ru, ^{116,118,120}Pd, ^{122,124,126,128}Cd, ^{130,132,134}Sn, ^{136,138}Te, ^{140,142,144}Xe, and ^{146,148}Ba. For all of them we computed the spheroidal prolate deformations by minimizing the deformation energy. When two colliding heavy ions come in contact, the energetically favored configuration is the tip-to-tip one, in which the two nuclei have elongated shapes along the internuclear axis. Therefore, these deformations were considered to be unchanged in the external region up the configuration in which the nuclei arrive in contact. The α-decay process was investigated from the microscopical point of view. Now, the work of [15] is extended by determining the least action trajectory for the fission process. The probabilities of disintegrations for α decay and for fission are reported for different values of the excitation energy of the compound nucleus.

2. FORMALISM

The half-life T for a spontaneous decay is calculated with the formula

$$T_s(E_v) = \frac{\ln 2}{\nu P(E_v)}, \tag{1}$$

where $\nu = \omega/2\pi$ is the frequency of assaults on the barrier, and

$$P(E_v) = \exp\left\{-\int \frac{2}{\hbar}\sqrt{2B[V-E_v]}dr\right\} \tag{2}$$

is the penetrability of the barrier. The integral is calculated between the turning points of the potential barrier determined by the vibration energy E_v. The angular velocity and the vibration energy are proportional, $E_v = \hbar\omega/2$. The zero point vibration energy is denoted E_0, being the lowest value of the collective kinetic energy of the system. If the system possesses an initial collective kinetic energy E_k, the vibration energy will be $E_v = E_k + E_0$. By considering E_v in MeV units, the half-life in s units is simply

$$T_s(E_v) = \frac{1.433 \times 10^{-21}}{E_v P(E_v)}. \tag{3}$$

The superheavy nucleus is obtained as a consequence of a fusion reaction. Therefore, the compound system is always excited. Statistically, by assuming a thermalization of the initial nucleus, the excitation energy E^* can be shared equiprobably between the collective kinetic energy E_k and the intrinsic one E_p. So, the half-life of the system at the excitation energy E^* is defined as

$$\frac{1}{T} = \frac{\int_0^{E^*} \frac{1}{T_s(E_k+E_0)}\rho(E^*-E_k)dE_k}{\int_0^{E^*}\rho(E^*-E_k)dE_k}, \tag{4}$$

where $\rho(E)$ is the nuclear levels density at the energy E of the compound nuclear system. In our work, the nuclear levels density is obtained within the Gilbert-Cameron formula [16], similarly as in Ref. [17].

In order to calculate the penetrability (2), the deformation energy and the inertia along a fission path are required. We use an axial symmetric nuclear shape that offers the possibility to obtain a transition from one initial nucleus to the separated fragments. This parametrization is obtained by smoothly joining two spheroids of semi-axes a_i and b_i (i=1,2) with a neck surface generated by the rotation of a circle of radius R_3 around the axis of symmetry. By imposing the condition of volume conservation we are left with five independent generalized coordinates $\{q_i\}$ (i=1,5) that can be associated to five degrees of freedom: the elongation R given by the distance between the centres of the spheroids, the necking parameter $C_3 = S/R_3$ related to the curvature of the neck, the eccentricities i associated with the deformations of the nascent fragments, and the mass asymmetry parameter $\eta = a_1/a_2$. Alternatively, the mass asymmetry can be characterized also by the mass number of the light fragment A_2. This number is obtained by considering that the sum of the volumes of two virtual ellipsoids characterized by the mass asymmetry parameter η and the eccentricities ϵ_i (i=1,2) gives the volume of the parent. This parametrization was widely used by the Bucharest group in the calculations addressing the cluster

and alpha decay [15, 18–22], the fission process [23, 24], the dissipation during the decay [25–27], the pair breaking [28], the generalization of time dependent pairing equations [29], and the heavy element synthesis [30, 31].

A Woods-Saxon mean field potential is associated to the nuclear shape parametrizations described above. The single-particle wave functions of this mean field are obtained in a single Hermite space by using the two-center prescriptions. The many-body wave function and the single particle energies are provided by the Woods-Saxon two-center shell model [29]. The Woods-Saxon potential, the Coulomb interaction and the spin orbit term must be diagonalized in an eigenvector basis. A complete analytical eigenvector basis can be only obtained for the semi-symmetric two-center oscillator. This potential corresponds to a shape parametrization given by two ellipsoids that possess the same semi-axis perpendicular on the axis of symmetry. The potential is

$$V_o(\rho,z)=\begin{cases}\frac{1}{2}m\omega_{z1}^2(z-c_1)^2+\frac{1}{2}m\omega_\rho^2, & z<0,\\ \frac{1}{2}m\omega_{z2}^2(z-c_2)^2+\frac{1}{2}m\omega_\rho^2, & z\geq 0,\end{cases} \tag{5}$$

where ω denotes the stiffness of the potential along different directions as follows, $\omega_{z1}=\omega_0\frac{R_0}{a_1}$, $\omega_{z2}=\omega_0\frac{R_0}{a_2}$, $\omega_\rho=\omega_0\frac{R_0}{b_1}$, $\omega_0=41A_0^{-1/3}$, $R_0=r_0A_0^{1/3}$, in order to ensure a constant value of the potential on the surface. The origin on the z-axis is considered as the location of the plane of intersection between the two ellipsoids. The asymmetric two-center shell oscillator provides an orthogonal eigenvector basis. For reflection-symmetric shapes, the solutions along the z-axis are also characterized by the parity as a good quantum number. The prescriptions for the two-center model are inspired from Refs. [32–34].

3. RESULTS

To obtain the macroscopic-microscopic barriers, a minimization of the energy is searched for all paths connecting the ground state and the fission valley as specified for example in Ref. [35]. The energy is obtained by using a dense grid points inside the available deformation space. Different fission trajectories are prospected in the configuration space, starting from the ground state of the compound nucleus and reaching the exit point from the potential barrier. The best trajectory is obtained when the following functional

$$P=\exp\int_{r_a}^{r_b}\frac{2}{\hbar}\sqrt{B(s)E(s)}ds \tag{6}$$

is minimized. In the previous expression, the first turning point r_a is at the equilibrium deformation while the second one r_b lies on the equipotential curve of the same deformation energy as the ground state that defines the exit of the barrier. $B(s)$ is the

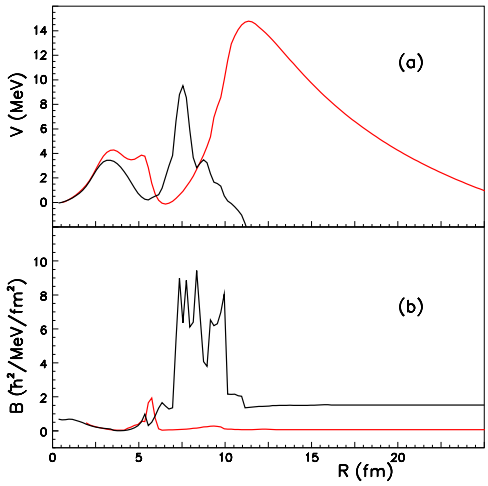

Fig. 1 – (Color online) (a) The potential barrier for the near-symmetric fission process is plotted with a black curve while the potential barrier for the α decay is plotted with a red one. The barriers are represented as function of the distance between the centers of the fragments R. (b) The effective masses for the fission process and the α decay are plotted with the same colors as in the panel (a).

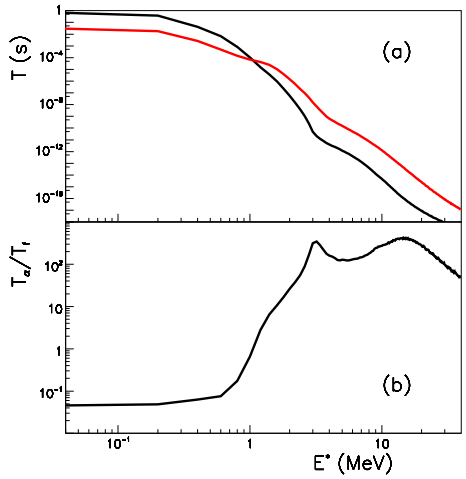

Fig. 2 – (Color online) (a) The half-lives T are plotted as function of the excitation energy E^* of the compound nucleus. The black curve represents the behavior for the near-symmetric fission process while the red one is for the α decay. (b) Ratio between the partial half-lives of the α-decay and the fission process.

inertia along the fission trajectory

$$B(s) = \sum_{i,j} B_{q_i q_j} \frac{\partial q_i}{\partial s} \frac{\partial q_j}{\partial s} \tag{7}$$

where $B_{q_i q_j}$ are the elements of the effective mass tensor as function of the deformation parameters q_i and q_j [36]. The motion is adiabatic. So, the flux in the fission channel is not redistributed in other degrees of freedom, as considered with complex potentials [37].

The fission of superheavy elements depends on the deformations of the two nascent fragments. The ground state is characterized by a nearly spherical shape stabilized by strong shell effects, the elongation being $R \approx$0 fm. Very small deviations from the quasispherical shapes produce rapid increase of the deformation energy. It is interesting to note that the fission trajectories for both channels, fission process and α decay, proceed initially through very compact configurations. Meaning, the nuclear shapes are obtained by a combination of two oblate spheroids joined by an intermediate necking region, for elongations R smaller than 3 fm. Around $R =$3 fm, the deformation energy reaches a maximum value, a first potential barrier being formed. After the passage of the first barrier, the path for the fission channel is now determined by a combination of two spheroids, which become to be prolate. After the top of the first barrier, the α decay proceeds along a valley in the deformation energy, where the asymmetry parameter increases. The potential barrier shapes of the α decay and of the fission process are represented in Fig. 1 (a) as function of the distance between the two nascent fragments. The inertia is displayed in Fig. 1 (b) for the same processes. It can be seen that asymptotically the inertia tends to reproduce the reduced masses of the two channels. The effective mass of the fission process is everywhere larger than that of the α decay. The height of the fission barrier is 9.02 MeV, being obtained by subtracting a zero point vibration energy of 0.5 MeV. The height of the fission barrier is of crucial importance for calculations of cross section for heavy or superheavy elements synthesis [38]. Using fission barriers evaluated dynamically, the half-lives of superheavy elements could be evaluated, as explained in Ref. [39]. This quantity was computed in Ref. [40] giving a value of 6.4 MeV. From systematic investigation in the framework of the macroscopic-microscopic approach concerning the fission properties of heavy and superheavy nuclei, a value of the potential barrier of 9.1 MeV was obtained in Ref. [41], which agrees to the result presented in this work.

The partial half-lives of the two channels are calculated with Eq. (4) as function of the excitation energy of the compound nucleus. If the compound nuclear system arrives in its ground state without excitation energy, then the present evaluation predicts T_α=0.0887 s for the α decay and T_f=2.21 s for the fission process. Therefore, at very low excitation energies the α decay is the dominant channel in the disinte-

gration of the superheavy element, by about one order of magnitude. The half-lives decrease abruptly with the excitation energy, by about three orders of magnitude for only E^*=1 MeV. For excitation energies larger that 1.1 MeV, the disintegration of the compound nuclear system proceeds mainly though fission.

4. CONCLUSION

A simple model able to predict the competition between the α decay and the fission process as function of the excitation energy of superheavy elements is presented. Calculations are realized for the ^{296}Lv isotope. Calculations of the half-lives of the superheavy elements are also possible by inferring semi-empirical parametrizations [42–44]. The parametrizations offer a good systematics of the half-lives if the masses, the Q-values and the height of the fission barriers are provided by the experimental data. In the present predictions, all the ingredients required to compute the half-lives are obtained from theory, without using additional parameters.

Acknowledgements. Work supported by the NUCLEU project number PN 19 06 01 01 /2019-2022.

REFERENCES

1. A. Sandulescu, R.K. Gupta, W. Scheid, and W. Greiner, Phys. Lett. B **60**, 225 (1976).
2. R.K. Gupta, C. Parvulescu, A. Sandulescu, and W. Greiner, Z. Phys. A **283**, 217 (1977).
3. R.K. Gupta, A. Sandulescu, and W. Greiner, Phys. Lett. B **67**, 257 (1977).
4. R.K. Gupta, A. Sandulescu, and W. Greiner, Z. Naturforsch **32**a, 704 (1977).
5. A. Sandulescu, D.N. Poenaru, and W. Greiner, Sov. J. Part. Nucl. **11**, 528 (1980).
6. Y.T. Oganessian *et al.*, Nucl. Phys. A **734**, 109 (2004).
7. Y.T. Oganessian *et al.*, Phys. Rev. Lett. **108**, 022502 (2012).
8. Y.T. Oganessian *et al.*, Phys. Rev. C **69**, 021601(R) (2004).
9. Y. Oganessian, J. Phys. G **34**, R165 (2007).
10. S. Hofmann and G. Munzenberg, Rev. Mod. Phys. **72**, 733 (2000).
11. S. Hofmann, G. Munzenberg, and M. Schadel, Nucl. Phys. News **14**, 5 (2004).
12. S. Hofmann, Rom. J. Phys. **57**, 214 (2012).
13. M.G. Itkis *et al.*, Int. J. Mod. Phys. E **16**, 957 (2007).
14. E.M. Kozulin *et al.*, Phys. Lett. B **686**, 227 (2010).
15. A. Sandulescu, M. Mirea, and D.S. Delion, EPL **101**, 62001 (2013).
16. A. Gilbert and A. G. W. Cameron, Can. J. Phys. **43**, 1446 (1965).
17. H.C. Britt, S.C. Burnett, B.H. Erkkila, J.E. Lynn, and E. Stein, Phys. Rev. C **4**, 1444 (1971).
18. M. Mirea, Phys. Rev. C **96**, 064607 (2017).
19. M. Mirea, EPL **124**, 12001 (2018).
20. M. Mirea, A. Sandulescu, and D.S. Delion, Nucl. Phys. A **870**, 23 (2011).
21. M. Mirea, A. Sandulescu, and D.S. Delion, Eur. Phys. J. A **48**, 85 (2012).
22. M. Mirea, Eur. Phys. J. A **51**, 36 (2015).

23. M. Mirea, Phys. Rev. C **89**, 034623 (2014).
24. M. Mirea, Int. J. Mod. Phys. E **27**, 1850076 (2018).
25. M. Mirea, Phys. Rev. C **83**, 054608 (2011).
26. M. Mirea, Phys. Lett. B **717**, 252 (2012).
27. M. Mirea and A. Sandulescu, Rom. Rep. Phys. **70**, 201 (2018).
28. M. Mirea Phys. Lett. B **680**, 316 (2009).
29. M. Mirea, Phys. Rev. C **78**, 044618 (2008).
30. M. Mirea, D. S. Delion, and A. Sandulescu, EPL **85**, 12001 (2009).
31. A. Sandulescu and M. Mirea, Eur. Phys. J. A **50**, 110 (2014).
32. J. Maruhn and W. Greiner, Z. Phys. **251**, 431 (1972).
33. E. Badralexe and A. Sandulescu, St. Cerc. Fiz. **25**, 1087 (1973).
34. E. Badralexe, M. Rizea, and A. Sandulescu, Rev. Roum. Phys. **19**, 63 (1974).
35. M. Brack, J. Damgaard, A. S. Jensen, H. C. Pauli, V. M. Strutinsky, and C. Y. Wong, Rev. Mod. Phys. **44**, 320 (1972).
36. M. Mirea, J. Phys. G **43**, 105103 (2016).
37. M. Mirea, Rom. J. Phys. **64**, 305 (2019).
38. K.-H. Schmidt and W. Morawek, Rep. Prog. Phys. **54**, 949 (1991).
39. R. Smolanczuk, J. Skalski, and A. Sobiczewski, Phys. Rev. C **52**, 1871 (1995).
40. I. Muntian, Z. Patik, and A. Sobiczewski, Acta Phys. Polonica B **34**, 2141 (2003).
41. P. Moller, A.J. Sierk, T. Ichikawa, A. Iwamoto, R. Bengtsson, H. Uhrenholt, and S. Aberg, Phys. Rev. C **79**, 064304 (2009).
42. C.I. Anghel, I. Silisteanu, and M. Zadehrafi, Rom. Rep. Phys. **71**, 213 (2019).
43. I. Silisteanu and C.I. Anghel, Rom. J. Phys. **62**, 303 (2017).
44. A.O. Silisteanu, C.I. Anghel, and I. Silisteanu, Rom. J. Phys. **63**, 302 (2018).